Supporting Information

A Cu^{+}-specific CopB transporter: Revising P_{1B}-type ATPase classification

Rahul Purohit[a], Matthew O. Ross[a], Sharon Batelu[b], April Kusowski[b], Timothy L. Stemmler[b], Brian M. Hoffman[a], and Amy C. Rosenzweig[a,1]

[a]Department of Molecular Biosciences and of Chemistry, Northwestern University, Evanston, Illinois, USA. [b]Department of Pharmaceutical Sciences, Wayne State University, School of Medicine, Detroit, Michigan, USA.

[1]To whom correspondence should be addressed. E-mail: amyr@northwestern.edu

Supporting Materials and Methods

Cloning, expression, and purification of *Sphaerobacter thermophilus* CopB constructs. The *Sphaerobacter thermophilus* DSM 20745 copper-transporting P-type ATPase (EMBL id: ACZ40742, Uniprot id: D1CA99) sequence was utilized to design a wildtype *S. thermophilus* P_{1B-3}-ATPase construct (WT-*St*CopB, residues 1-785) and a delta construct lacking the N-terminal MBD (ΔMBD-*St*CopB, residues 114-785). Codon-optimized versions of each gene with a C-terminal TEV-protease cleavage site (ENLYFQSAG) were synthesized by GenScript USA Inc. (Piscataway, NJ). Both genes were subcloned into the pET-21a(+) plasmid with a C-terminal hexa-histidine (His_6) tag using the NdeI and XhoI restriction sites. A tagless WT-*St*CopB construct without the C-terminal TEV-cleavage site and His_6 tag was generated by inserting a stop codon at the C-terminus of the protein sequence using the QuikChange site directed mutagenesis kit (Agilent). Mutants of ΔMBD-*St*CopB (C404A, H406A, H406C, M739A, C404A/H406A) were also generated using the QuikChange site directed mutagenesis kit. The *St*CopB-MBD gene, encoding residues 1-120, was cloned into a ligation-independent cloning (LIC) vector, pET StrepII TEV LIC (2R-T) (Addgene plasmid #29717), that adds an N-terminal TEV-protease cleavable Strep-II tag (MASWSHPQFEKGAENLYFQSNA). Briefly, the *St*CopB-MBD gene was PCR amplified from the genomic DNA template of *S. thermophilus* using forward primer 5′- tacttccaatccaatgcaagttcgacgccacagcat-3′ and reverse primer 5′-ttatccacttccaatgttattagcgccgtcggaagacgtc-3′ (LIC overhang residues are underlined). The PCR product was gel purified and then treated with excess dCTP and LIC-quality T4 DNA polymerase (Thermo Scientific). The vector was prepared for ligation by gel purifying the SspI (New England BioLabs) digested product and then treating the linearized product vector with dGTP and LIC-quality T4 DNA polymerase. Cloned product was obtained by mixing the vector

and insert in a ratio of 4:1 followed by incubation at 22 °C for 15 min in presence of 2.5 mM EDTA. The reaction mixture was then transformed into *E. cloni* 10G competent cells (Lucigen) and plated on 100 μg/ml ampicillin supplemented LB-agar plates.

WT-*St*CopB, ΔMBD-*St*CopB and ΔMBD-*St*CopB mutants (C404A, H406A, H406C, M739A, and C404A,H406A) were all expressed in *E. coli* strain BL21(DE3)-*ΔacrB*, which has the gene encoding the multidrug efflux pump AcrB disrupted and was obtained from the laboratory of Edward Yu at Iowa State University (1). Cells were grown at 37 °C to an OD_{600} of 0.8, induced with 1 mM isopropyl 1-thio-β-D-thiogalactopyranoside (IPTG), and then grown overnight at 18 °C for 18 h before harvesting by centrifugation at 4,800g for 15 min in a Sorvall SLC 4000 rotor at 4 °C. Cell pellets were flash frozen and stored at -80 °C until purification.

All purification steps were performed at 4 °C. Cell pellets were resuspended in resuspension buffer (25 mM Tris buffer, pH 7.5, 100 mM sucrose) supplemented with 10 mM EDTA, 1 mM phenylmethanesulfonyl fluoride (PMSF) and DNase I. Cells were disrupted using a microfluidizer and cell debris clarified by centrifugation for 45 min at 8000*g*. Cell membranes were isolated by ultracentrifugation for 1 h at 163,000*g* and then washed and homogenized in fresh resuspension buffer supplemented with 10 mM EDTA. Homogenized membranes were subjected to another round of ultracentrifugation and were again homogenized in resuspension buffer without EDTA. Clarified membranes containing *St*CopB proteins were solubilized with 1% *n*-dodecyl-β-D-maltopyranoside (DDM) (w/v) final detergent concentration, stirred at 4 °C for ~3 h, and then clarified by ultracentrifugation at 163,000*g* for 1 h. The supernatant was loaded onto two tandem 5-ml Ni^{2+}-loaded HiTrap Chelating HP columns (GE Healthcare) previously equilibrated with binding buffer (25 mM Tris, pH 7.5, 100 mM sucrose, 300 mM NaCl, 20 mM imidazole, 0.05% (w/v) DDM). The column was washed with 5 column volumes

(CVs) of binding buffer followed by another wash with 5 CVs of binding buffer containing 50 mM imidazole. Bound protein was eluted in two steps using 5 CVs of 150 mM imidazole-containing binding buffer and 5 CVs of 300 mM imidazole-containing binding buffer. Fractions containing WT-*St*CopB were pooled, supplemented with 5 mM EDTA, and concentrated using a 100 kDa MWCO Amicon spin concentrator (Millipore). WT-*St*CopB was further purified using a 120 mL Superdex 200 column size exclusion column (GE Healthcare) previously equilibrated with ATPase equilibration buffer (25 mM Tris buffer, pH 7.5, 100 mM NaCl, 50 mM sucrose, 0.02% DDM (w/v). The final material (typical yield 4-5 mg purified protein per L cell culture) was concentrated to 20 mg/mL using a 100 kDa spin concentrator and stored at −80 °C.

Cleavage of the C-terminal His_6 tag from ΔMBD-*St*CopB constructs was achieved by adding purified His_6-tagged TEV protease to the pooled ΔMBD-*St*CopB containing fractions followed by overnight dialysis at 4 °C against dialysis buffer 1 (25 mM Tris, pH 7.5, 50 mM NaCl, 0.01% DDM (w/v), 2 mM EDTA, 5 mM 2-mercaptoethanol (2-ME)). A second dialysis was performed against dialysis buffer 2 (25 mM Tris, pH 7.5, 100 mM NaCl, 0.01% DDM (w/v)). The dialyzed product was again loaded onto two tandem 5-ml Ni^{2+}-loaded HiTrap Chelating HP columns to remove the His_6-tagged TEV-protease. ΔMBD-*St*CopB samples were then concentrated, further purified on a Superdex 200 column, concentrated to ~20 mg/mL, and flash frozen.

*St*CopB-MBD was expressed in BL21 (DE3) cells in LB media supplemented with 100 μg/ml ampicillin. Cells were grown at 37 °C to an OD_{600} of 0.8, induced with 1 mM IPTG, and then grown overnight for 18 h at 18 °C before harvesting. Cell pellets were flash frozen and stored at -80 °C until purification. Cell pellets were resuspended in MBD resuspension buffer (25 mM Tris buffer, pH 7.5, 100 mM NaCl) supplemented with DNase I and 1 mM PMSF and were

disrupted using a sonicator. Cell debris and membranes were clarified by ultracentrifugation at 163,000g for 1 h. The supernatant was loaded onto two tandem 5-ml Ni^{2+}-loaded HiTrap Chelating HP columns previously equilibrated with MBD binding buffer (25 mM Tris buffer, pH 7.5, 100 mM NaCl, 5% glycerol, 20 mM imidazole). The column was washed with 5 column volumes (CVs) of MBD binding buffer followed by another wash with 5 CVs of MBD binding buffer containing 50 mM imidazole. Bound protein was eluted in two steps using 5 CVs of 150 mM imidazole-containing MBD binding buffer and 5 CVs of 300 mM imidazole-containing MBD binding buffer. Fractions containing *St*CopB-MBD were pooled, supplemented with 5 mM EDTA, and concentrated using a 10 kDa MWCO Amicon spin concentrator. The protein was further purified using a Superdex 75 size exclusion column (GE Healthcare) previously equilibrated with equilibration buffer (25 mM Tris, pH 7.5, 100 mM NaCl, 5% glycerol). Fractions containing the MBD (typical yield 3-4 mg purified protein per L cell culture) were pooled, concentrated, flash frozen, and stored at -80 °C. To confirm the identity of purified *St*CopB-MBD, mass spectrometry analyses were performed at Northwestern University Proteomics Core. Briefly, purified *St*CopB-MBD was ran on 15% SDS-PAGE and thin slices of bands corresponding to *St*CopB-MBD were excised from the gel. The sample was digested with trypsin, and peptides were analyzed using an LTQ Orbitrap Velos mass spectrometer.

Similar to *St*CopB, the *Archaeoglobus fulgidus* CopB (*Af*CopB) P-type ATPase sequence (EMBL id: AAB91079, Uniprot id: O30085) was utilized for generation of a codon-optimized full length construct (residues 1-690) that was commercially synthesized by GenScript USA Inc. (Piscataway, NJ) with a C-terminal TEV-protease cleavage site (ENLYFQSAG), and subcloned into the pET-21a(+) plasmid with a C-terminal hexa-histidine (His_6) tag using the NdeI and XhoI restriction sites. All purification steps were performed identical to the WT-*St*CopB purification.

Structure prediction and homology modeling. *St*CopB-MBD secondary structure prediction and disordered region prediction were obtained using PSIPRED and DISOPRED3, respectively (http://bioinf.cs.ucl.ac.uk/psipred/) (2). Homology models for *St*CopB-MBD (residues 1-120) and WT-*St*CopB (residues 1-785) were obtained using the Robetta Protein Structure Prediction Server (http://robetta.bakerlab.org/) (3, 4). The *St*CopB-MBD 3D structure prediction model was generated using *ab initio* modeling in the absence of any template structure, and full length *St*CopB was modeled based on the *Af*CopA cryo-EM model (5) (PDB ID 3J09).

Circular dichroism spectroscopy. Circular dichroism (CD) spectra were acquired from 185 nm to 245 nm with 1 nm spectral bandwidth using a Jasco J-815 spectropolarimeter at 20 °C. Apo *St*CopB-MBD was diluted to 0.1 mg/mL in CD buffer (10 mM sodium phosphate buffer, pH 7.4,10 mM NaF). Spectra were recorded in a 2 mm path length quartz cuvette with a scan speed of 20 nm/min and 16 s data integration time (D.I.T.) and represent the average of two accumulations. Spectra in the presence of 2,2,2-trifluoroethanol (TFE) were obtained by diluting apo *St*CopB-MBD in CD buffer containing 33% TFE. Scans of buffer alone were subtracted from the protein spectrum and plotted.

Metal loading and ICP-OES. *St*CopB constructs were diluted to ~20 μM in metal loading buffer (50 mM Tris buffer, pH 7.5, 500 mM NaCl, 20% glycerol, 0.05% DDM). Samples loaded with Cu^{2+}, Ni^{2+}, Zn^{2+}, Co^{2+}, and Ag^{+} were prepared by slow addition of 10 mol equiv of the metal ion over 1 h and incubation overnight at 4 °C while rocking gently. For variable Cu^{2+} loading assays, samples were prepared separately by adding 0.75, 1, 2, 5 and 10 equivalents of

copper provided as $CuCl_2$. Loading of Cu^+ was performed in a Coy anaerobic chamber by adding 2-3 equivalents of copper(I) tetrakis(acetonitrile) hexafluorophosphate ($[Cu(CH_3CN)_4]PF_6$) to the protein in metal loading buffer supplemented with 5 mM 2-mercaptoethanol (2-ME) and incubating for 1 h at room temperature. Controls for metal loading measurements were performed with no protein present in the reconstitution mixture. Excess copper was removed using an EconoPac 10DG desalting column (Bio-Rad) or a Zeba spin desalting column, and the protein was exchanged back into ATPase equilibration buffer containing 5 mM 2-ME. The protein was concentrated by using a 100 kDa MWCO Amicon spin concentrator, and the concentration was measured using the DC Lowry assay. Protein samples for metal analyses were prepared by digestion in 5 mL of 5% TraceSelect nitric acid (Sigma Aldrich). Multi-element calibration standards (Inorganic Ventures) were also diluted in 5% TraceSelect nitric acid. Protein metal contents were measured by using a Thermo-Fisher iCAP 7600 inductively coupled plasma optical emission spectrometer (ICP-OES, Quantitative Bioelement Imaging Center, Northwestern University), and are the average of three independent samples.

ATPase activity assay. Metal-dependent ATP hydrolysis activity of *St*CopB constructs was measured using the malachite green assay (6) as described previously (7). Briefly, malachite green assay reagent was prepared fresh by mixing 4.2% ammonium molybdate tetrahydrate (prepared in 4 M HCl) and 0.045% malachite green carbinol (prepared in water) in a 3:1 (v/v) ratio and stirring for at least 20 min before filtering. *St*CopB proteins were diluted to ~0.01-0.02 mg/mL using stock buffer with a final composition of 50 mM Tris, pH 7.5, 3 mM $MgCl_2$, 200 mM NaCl, 0.1 mg/mL asolectin as source of lipids, and 0.01% (w/v) DDM. Metal-stimulated activity was tested by the addition of stock metal salts ($CoCl_2$, $NiCl_2$, $CuCl_2$, $ZnCl_2$ and $AgNO_3$)

to a final concentration of 10 μM. Assays for Cu^{+}-stimulated activity were performed by in situ generation of Cu^{+} from Cu^{2+} reduction in the presence of 2.5 mM 2-ME. When testing reducing agents, 2.5 mM DTT, 2.5 mM TCEP, 20 mM cysteine, or 20 mM sodium ascorbate were included in the reaction. ATPase activity inhibition by sodium orthovanadate was tested at 1 mM concentration, and inhibition by bathocuproinedisulfonic acid disodium salt (BCS) (Sigma-Aldrich) was tested at 1 mM concentration in the reaction. ATP-disodium salt was used as the substrate, and the hydrolysis reaction was carried out in 1.5 mL Eppendorf tube at 55 °C with 1000 rpm shaking for 10-15 min. The reaction was stopped by addition of the malachite green reagent, and color development was stabilized by addition of a 34% stock solution of sodium citrate to a final concentration of 3.1% (v/v). The absorbance at 660 nm was measured using an Agilent 8453 spectrophotometer. A stock solution of K_2HPO_4 was used to generate an inorganic phosphate standard curve. Specific activity data are corrected against background hydrolysis of ATP in the absence of enzyme ± metal cations. BCS-Cu^{+} complex formation was tested by addition of 25 μM $CuCl_2$ to 100 μM BCS followed by addition of different reducing agents in excess, and monitoring of complex formation by the absorbance at 480 nm.

Electron paramagnetic resonance (EPR) spectroscopy. WT-*St*CopB and ΔMBD-*St*CopB EPR samples were prepared in ATPase buffer at protein concentrations of 0.1-0.4 mM. X-band and Q-band samples were frozen in liquid nitrogen in Wilmad quartz EPR tubes (Sigma Aldrich) and custom quartz Q-band tubes, respectively, and stored until analysis. Continuous wave (CW) X-band spectra were measured on a Bruker ESP-300 spectrometer using an Oxford Instruments ESR-900 helium flow cryostat. X-band spectra were normalized to gain and protein concentration, as well as background corrected by subtraction of a 50 mM Tris pH 8.0, 150 mM

NaCl EPR spectrum. CW Q-band EPR and ENDOR spectra were collected at 2 K under rapid adiabatic passage conditions using a spectrometer described elsewhere (8).

X-ray absorption spectroscopy. WT-*St*CopB samples loaded with Cu^{+} were prepared anaerobically as described above in 25 mM Tris, pH 7.5, 100 mM NaCl, 0.02% DDM, 5 mM 2-ME, and 30% glycerol with final copper concentrations of 0.4−0.6 mM. ΔMBD-*St*CopB samples loaded with Cu^{2+} were prepared as described above. Two independent replicates of copper-loaded WT-*St*CopB and ΔMBD-*St*CopB samples were prepared and loaded into 2 mm Lucite cells wrapped with Kapton tape. Samples were flash frozen and stored in liquid nitrogen until data collection. XAS data were collected at the Stanford Synchrotron Radiation Laboratory (SSRL) on beamline 9-3 using a Si(220) double crystal monochromator equipped with a harmonic rejection mirror. Samples were maintained at 10 K using Oxford Instruments continuous-flow liquid helium cryostat. Protein fluorescence excitation spectra were collected using a 100-element Ge solid-state array detector. A nickel filter (0.6 μM in width) and solar slits were placed between the cryostat and detector to filter scattering fluorescence not associated with protein Cu signals. XAS spectra were measured using 5 eV steps in the pre-edge region (8750-8960 eV), 0.25 eV steps in the edge region (8986-9050 eV), and 0.05 $Å^{-1}$ increments in the extended X-ray absorption fine structure (EXAFS) region (to k = 13.5 $Å^{-1}$), integrating from 1 to 20 seconds in a k^3 weighted manner for a total scan length of approximately 40 min. X-ray energies in the protein spectra were calibrated by collecting simultaneous Cu foil absorption spectra, assigning the first inflection point in the foil spectra as 8980.3 eV. Each fluorescence channel of each scan was examined for spectral anomalies prior to averaging and spectra were closely monitored for any photodamage. Slight photoreduction was observed in the second scan

at each exposure position. Thus, to quantitate the extent and impact of photoreduction, individual spectra were collected at unique positions on the sample surface (ensuring new face for radiation exposure), and only the initial exposure spectrum at each sample position was used during the overall data analysis. Data represent the average of 6 scans.

XAS data were processed using the Macintosh OS X version of the EXAFSPAK program suite (http://ssrl.slac.stanford.edu/exafspak.html) integrated with the Feff v8 software (9) for theoretical model generation. Data reduction followed a previously published protocol for a spectral resolution in bond lengths of 0.13 Å (10). EXAFS fitting analysis was performed on raw/unfiltered data. Protein EXAFS data were fit using single scattering Feff v8 theoretical models, calculated for possible Cu-carbon, oxygen, sulfur and copper coordination environments, with values for the scale factors (Sc) and E_0 calibrated by fitting crystallographically characterized copper model compounds, as outlined previously (10). Criteria for judging the best-fit EXAFS simulations utilized both the lowest mean square deviation between data and fit corrected for the number of degrees of freedom (*F'*) (11) and reasonable Debye-Waller factors ($\sigma^2 < 0.006$ Å^2)(12).

Sequence similarity network generation. The sequence similarity network (SSN) for P_{1B}-ATPases was generated by using the web-based Enzyme Function Initiative-Enzyme Similarity Tool (EFI-EST)(13) and visualized with Cytoscape(14). The NCBI BLAST web server was used to search for new sequences containing CPG (250 sequences) and SCSC (22 sequences) motifs in helix TM4. These new sequences in FASTA format were merged with sequences from a previously generated P_{1B}-ATPase sequence database(15). All FASTA formatted sequences were then analyzed for similarity by performing all-by-all BLAST using the EFI-EST webserver

(http://efi.igb.illinois.edu/efi-est/)(13) with a default E-value of 5. An alignment score of 125 (~45% sequence identity) was then used to create the SSN. Individual protein sequences, termed nodes, and lines connecting two nodes, termed edges, were visualized using the Cytoscape tool (v3.5.1) (14) with organic layout. The SSN was then filtered within Cytoscape to show edges corresponding to 35% sequence identity. Individual nodes were colored based on the presence of different conserved TM4 motifs.

Supporting Figures

Fig. S1. Sequence alignment of CopB MBDs. Sequences from *Aquifex aeolicus* copper transporter (*Aa*CtrA3, Uniprot ID: O67203), *Sphaerobacter thermophilus* CopB (*St*CopB, Uniprot ID: D1CA99), *Thermus thermophilus* CopB (*Tt*CopB, Uniprot ID: Q5SHJ7), *Nostoc sp.* CopB (*Ns*CopB, Uniprot ID: K9QPQ2), *Enterococcus hirae* CopB (*Eh*CopB, Uniprot ID: P05425), *Archaeoglobus fulgidus* CopB (*Af*CopB, Uniprot ID: O30085), and *Methanosarcina acetivorans* CopB (*Ma*CopB, Uniprot ID: Q8TUA7) were aligned using JalView (v. 2.10) implementing the ClustalO algorithm.

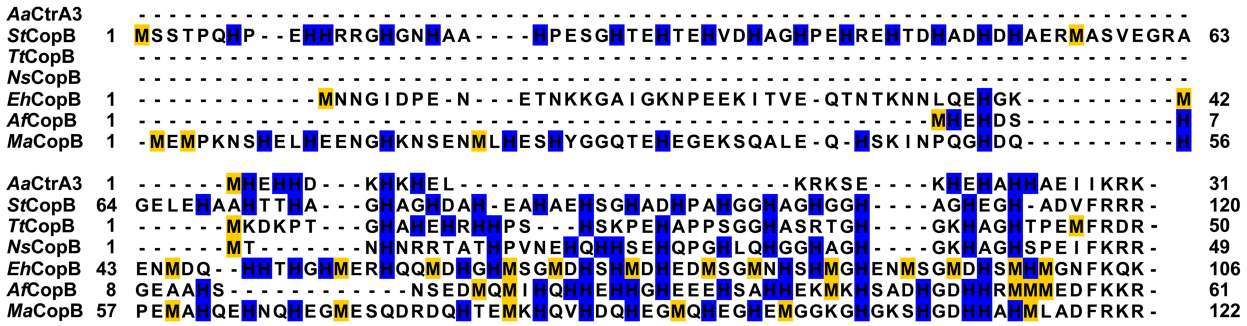

Fig. S2. (*A*) Schematic representation of the *St*CopB constructs used in this study. The approximate locations of the N-terminal MBD, TM helices, actuator domain (AD), ATP-binding domain (ATPBD), and affinity tags are labeled along with strictly conserved residues in TM helices. A C-terminal region containing a conserved HXHG motif sequence spans residues 751-785. (*B*) SDS-PAGE (12.5%) analysis of purified WT-*St*CopB, ΔMBD-*St*CopB, and *St*CopB-MBD (gel on left) and of membrane-bound *Af*CopB and purified *Af*CopB (gel on right). Molecular weight ladders are located on the left of each gel.

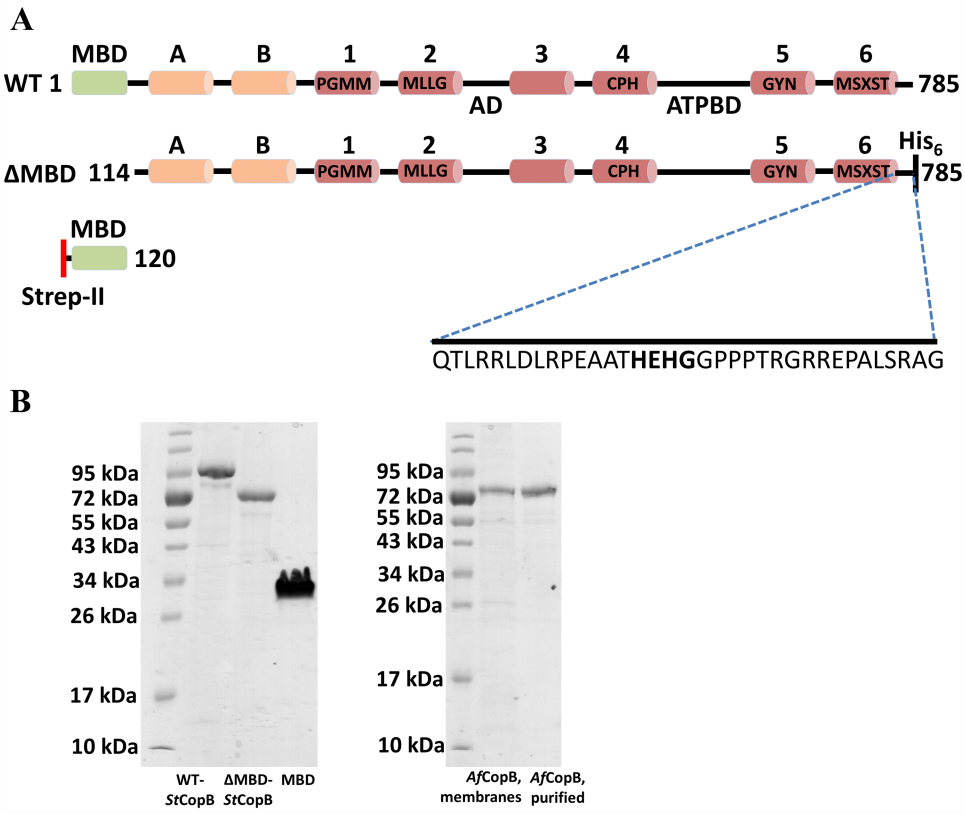

Fig. S3. Paramagnetic spectroscopic characterization of Cu^{2+}-bound ΔMBD-*St*CopB and full-length WT-*St*CopB proteins. **(***A***)** Top left: CW Q-band ΔMBD-*St*CopB absorption-display EPR. Bottom left: ^{14}N ENDOR measured near $g_{||}$, where the closed circle represents one half the hyperfine coupling and the goalpost width corresponds to twice the ^{14}N Larmor frequency. Right: ^{1}H ENDOR at $g_{\perp}$ (top) and $g_{||}$ (bottom), where the triangle represents the ^{1}H Larmor frequency and the goalposts indicate the ^{1}H hyperfine coupling, which is consistent with a directly coordinated H_xO ligand. For both ^{14}N and ^{1}H ENDOR, the red spectra depict frequency swept from low to high while black depict frequency swept from high to low. EPR conditions: 34.819 GHz microwave frequency, 64 ms time constant, 2 G modulation amplitude, ~2 min per scan, 4 total scans, temperature 2 K; ^{14}N ENDOR conditions: 34.833 GHz microwave frequency, 64 ms time constant, 1 G modulation amplitude, 0.5 MHz/s scan rate, 100 scans, temperature 2 K; ^{1}H ENDOR conditions: 34.822 GHz microwave frequency, 32 ms time constant, 2 G modulation amplitude, 0.75 MHz/s scan rate, at least 60 scans, temperature 2 K. **(***B***)** CW X-band EPR spectra of ΔMBD-*St*CopB and mutants thereof, and **(***C***)** spectra of WT-*St*CopB incubated with 0-10 Cu^{2+} equiv overnight then desalted to remove unbound Cu^{2+}. The C404A,H406A ΔMBD-*St*CopB sample was prepared in a Q-band tube, which was then placed in an X-band tube to measure the X-band EPR spectrum. All ΔMBD-*St*CopB spectra were scaled to unity. Conditions: 9.36-9.37 GHz microwave frequency, 320 ms time constant, 16 G modulation amplitude, 80 s scan time, and temperature 20 K.

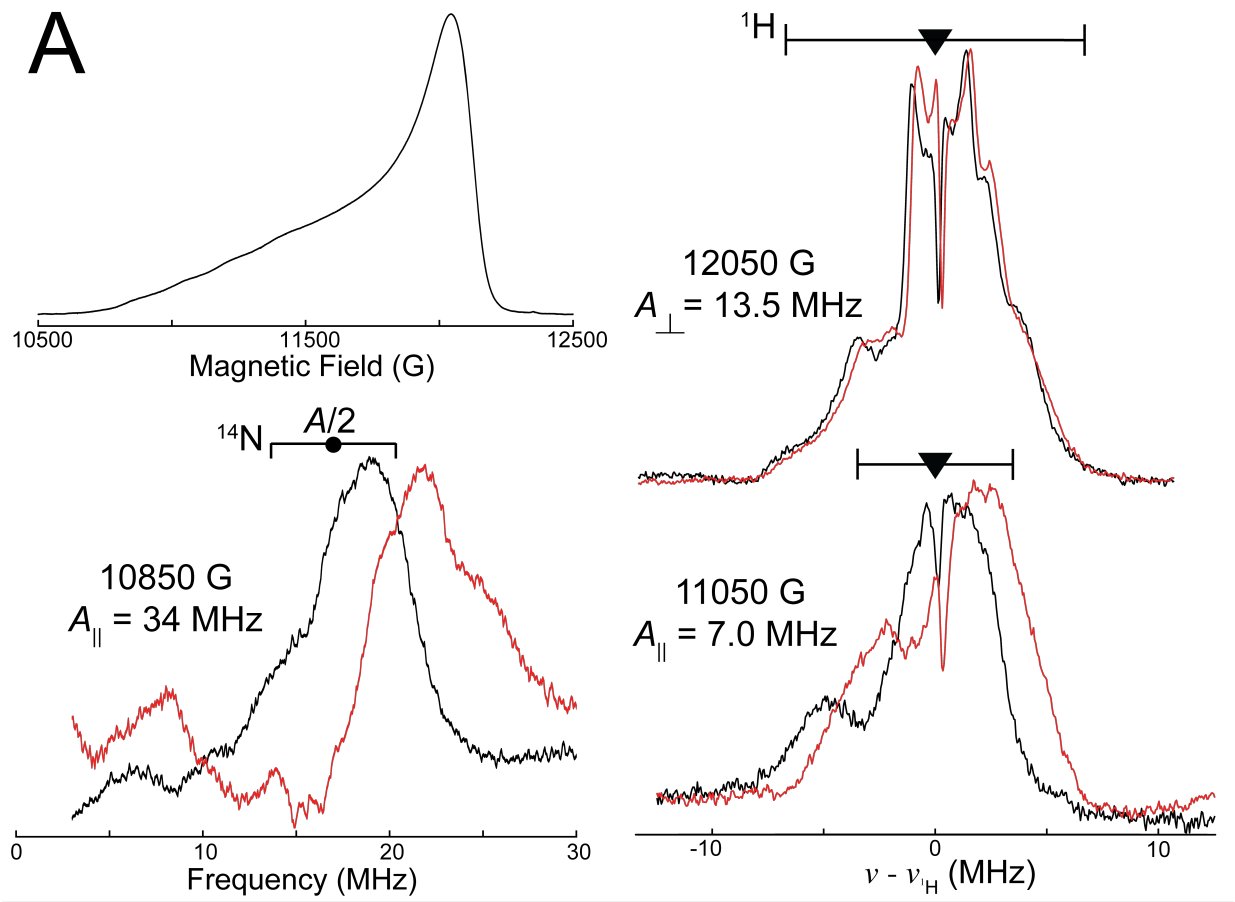
A
10500
11500
12500
Magnetic Field (G)
^{14}N
A/2
10850 G
$A_{||}$ = 34 MHz
0
10
20
30
Frequency (MHz)
^{1}H
12050 G
$A_{\perp}$ = 13.5 MHz
11050 G
$A_{||}$ = 7.0 MHz
-10
0
10
ν - $\nu_{^1H}$ (MHz)

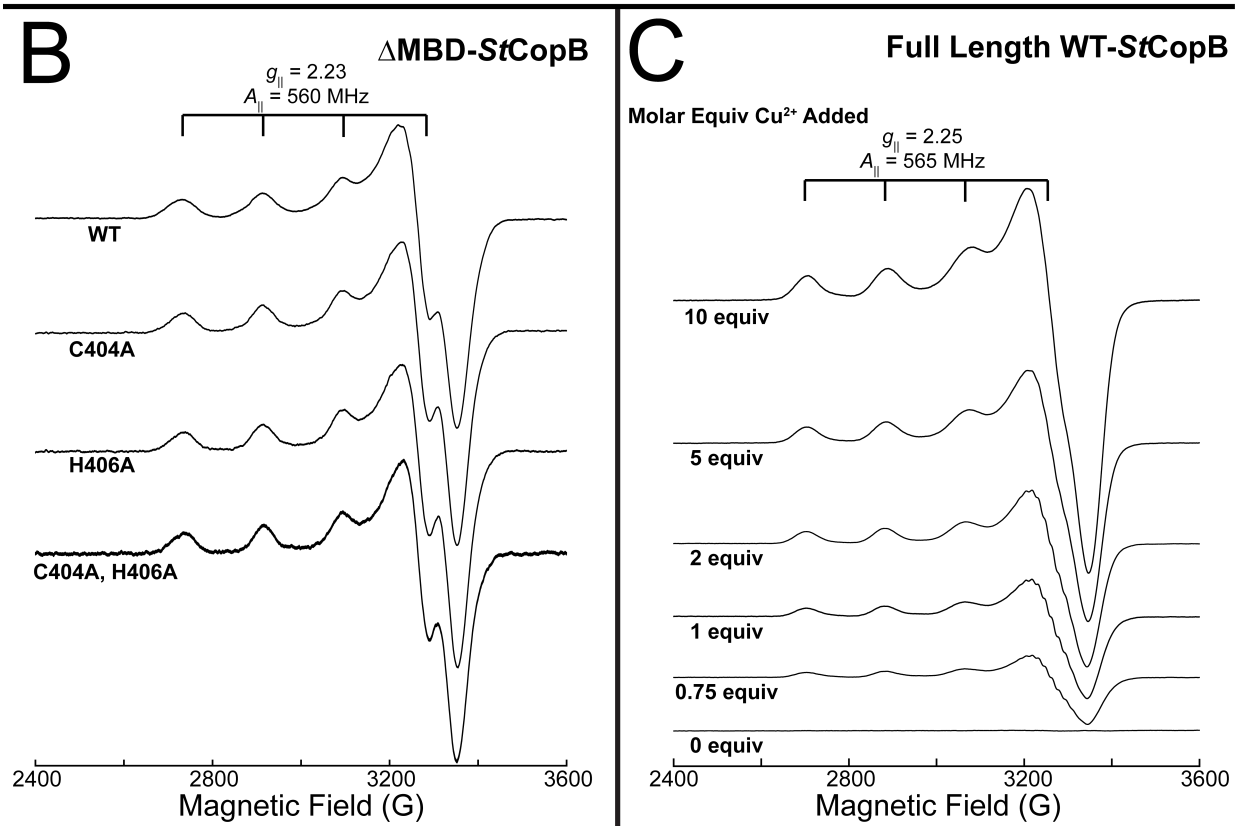
B
ΔMBD-StCopB
$g_{||}$ = 2.23
$A_{||}$ = 560 MHz
WT
C404A
H406A
C404A, H406A
2400
2800
3200
3600
Magnetic Field (G)
C
Full Length WT-StCopB
Molar Equiv Cu²⁺ Added
$g_{||}$ = 2.25
$A_{||}$ = 565 MHz
10 equiv
5 equiv
2 equiv
1 equiv
0.75 equiv
0 equiv
2400
2800
3200
3600
Magnetic Field (G)

Fig. S4. *St*CopB Robetta model (magenta) and LpCopA structure (PDB:3RFU, cyan) superimposed with an RMSD of 1.44 Å.

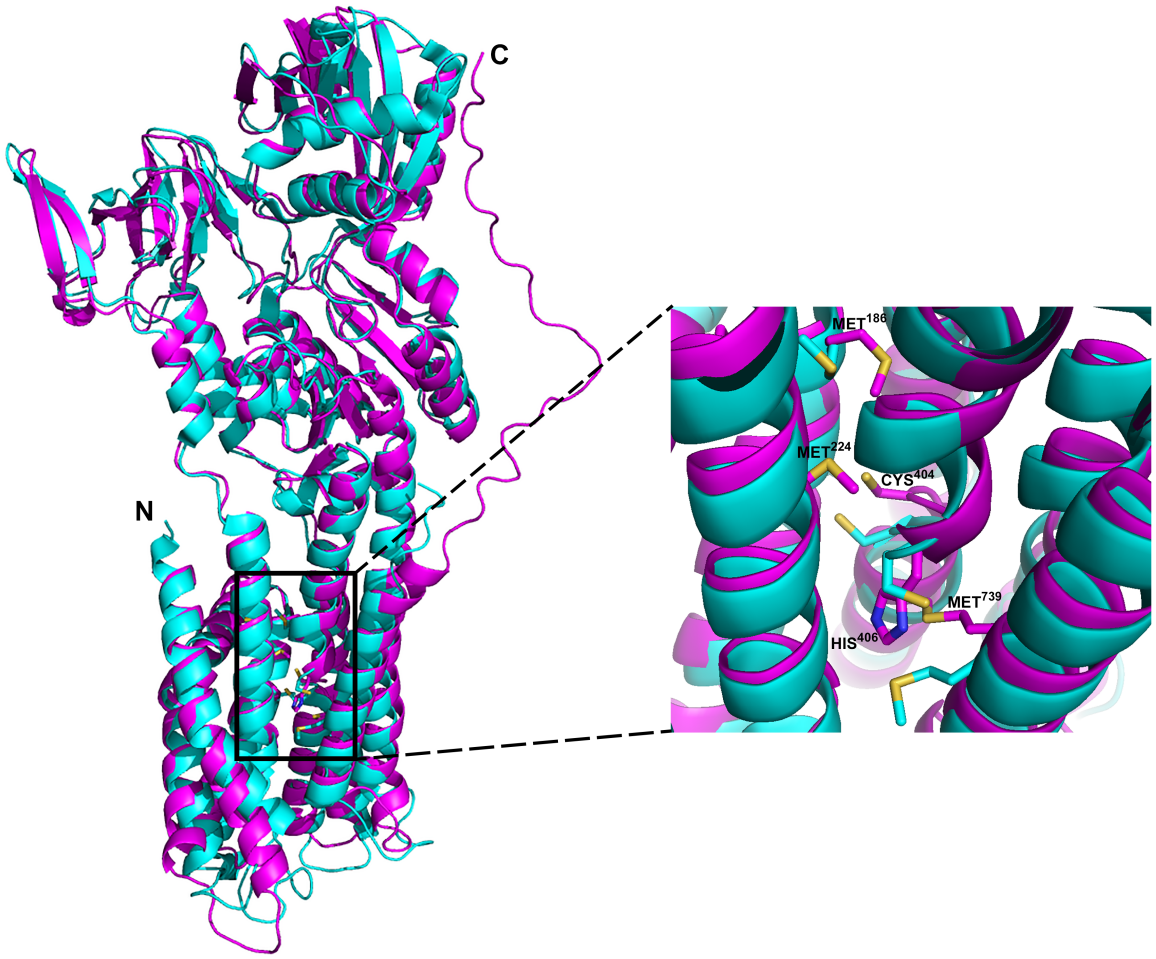

Fig. S5. Cu^{2+} (*A*) and Zn^{2+} (*B*) binding by WT-*St*CopB. Samples were reconstituted with varying amounts of Cu^{2+} or Zn^{2+} followed by desalting to remove unbound metal ions. The metal content was determined using ICP-OES. Each data point represents the average and standard deviation of three individual sample reconstitutions.

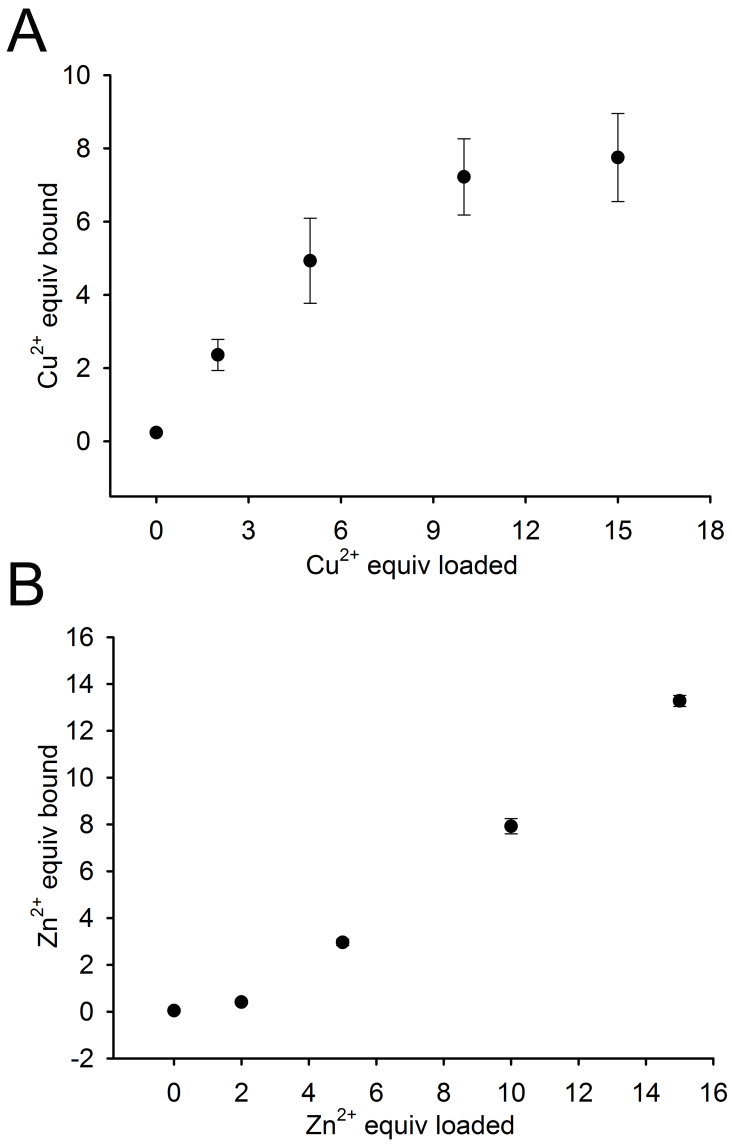

Fig. S6. (*A*) *St*CopB-MBD secondary structure prediction using the PSIPRED server (http://bioinf.cs.ucl.ac.uk/psipred/) indicating disordered regions in the MBD. (*B*) *St*CopB-MBD structure prediction models (magenta) were generated by *ab initio* modeling in the absence of any template structure using the Robetta Protein Structure Prediction Server (http://robetta.bakerlab.org/). The *St*CopB-MBD is only predicted to fold in the modeled full length *St*CopB (wheat).

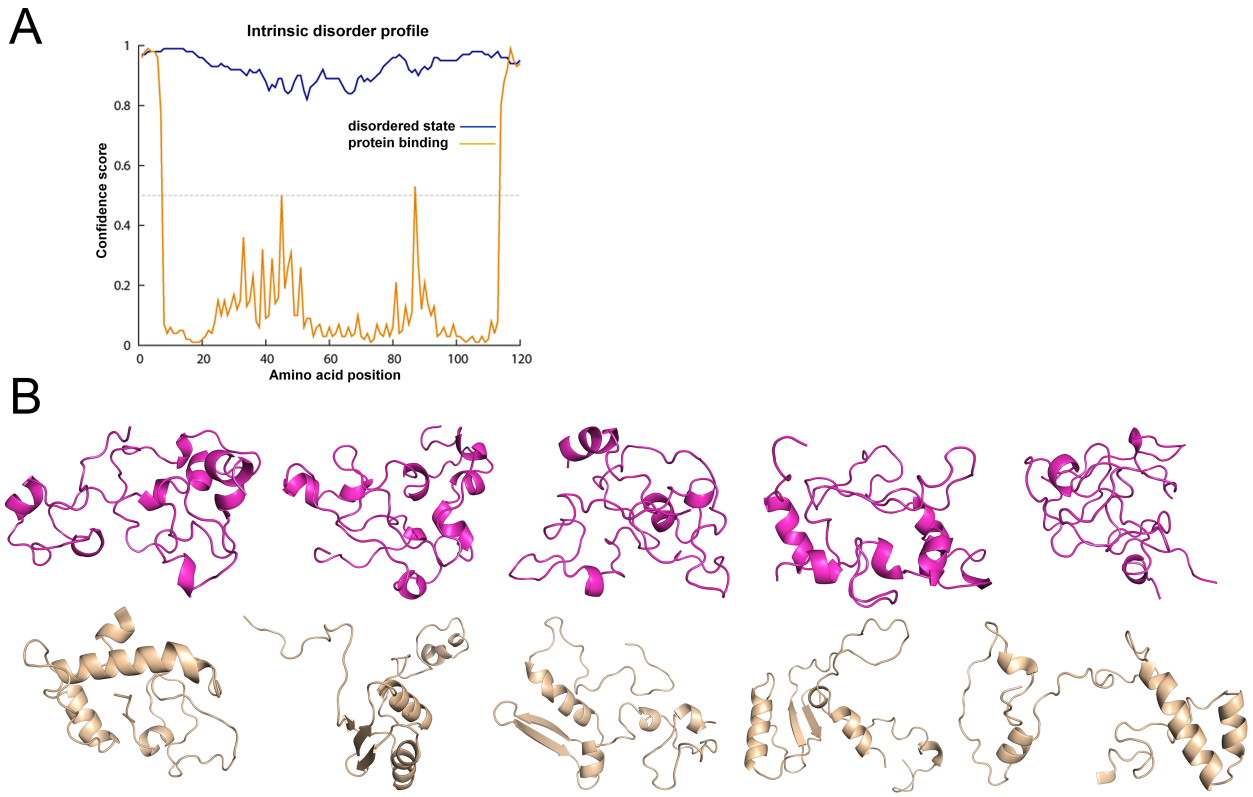

Fig. S7. Circular dichroism (CD) spectroscopic analysis of *St*CopB-MBD. The CD spectrum of *St*CopB-MBD shifts from a random-coil CD spectral signal (mdeg) at 198 nm to a folded helical spectral signal with minima at 208 nm and 222 nm upon addition of 33% TFE.

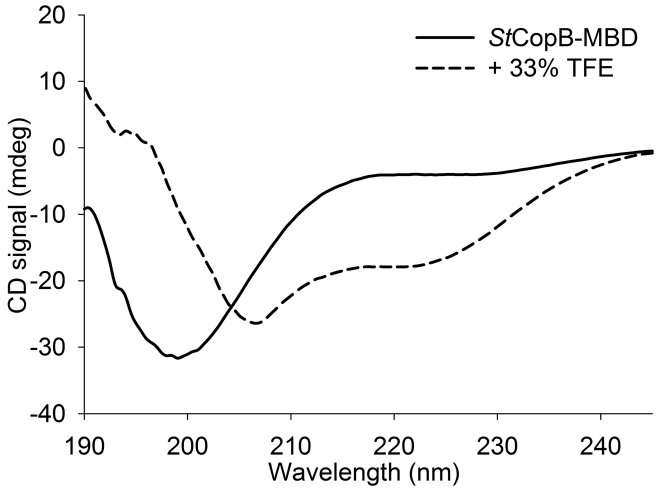

Fig. S8. Copper reduction by various reducing agents and formation of Cu^{+}-BCS complex monitored by absorbance at ~485 nm. DTT, TCEP and 2-ME were added to a final concentration of 2.5 mM and ascorbate and cysteine to a final concentration of 20 mM. The concentrations of $CuCl_2$ and BCS were 25 µM and 100 µM, respectively.

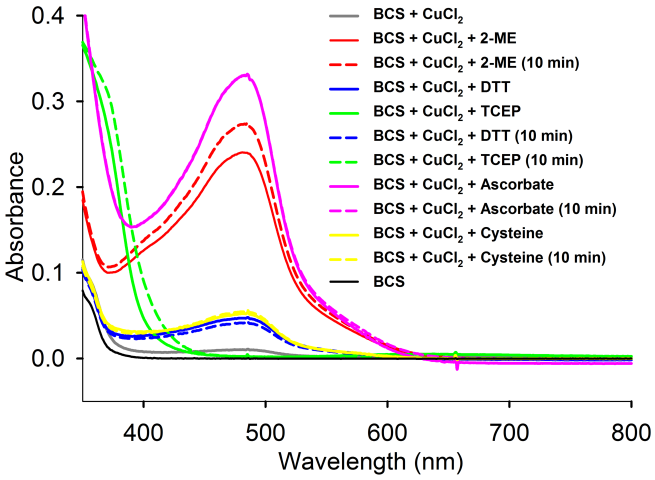

Fig. S9. X-ray absorption spectroscopic analysis of Cu^{2+}-loaded ΔMBD-*St*CopB samples and variants. Left, normalized K-edge Cu XANES spectra of ΔMBD-*St*CopB (black), variant C404A (red), and variant H406A (green). Right, raw and simulated EXAFS for ΔMBD-*St*CopB (A), variant C404A (C) and variant H406A (E) and Fourier transforms for ΔMBD-*St*CopB (B), variant C404A (D) and variant H406A (F) shown in respective panels. Simulated data is given in green while raw data is shown in black. The EXAFS fits are shown in Supplementary Table 3.

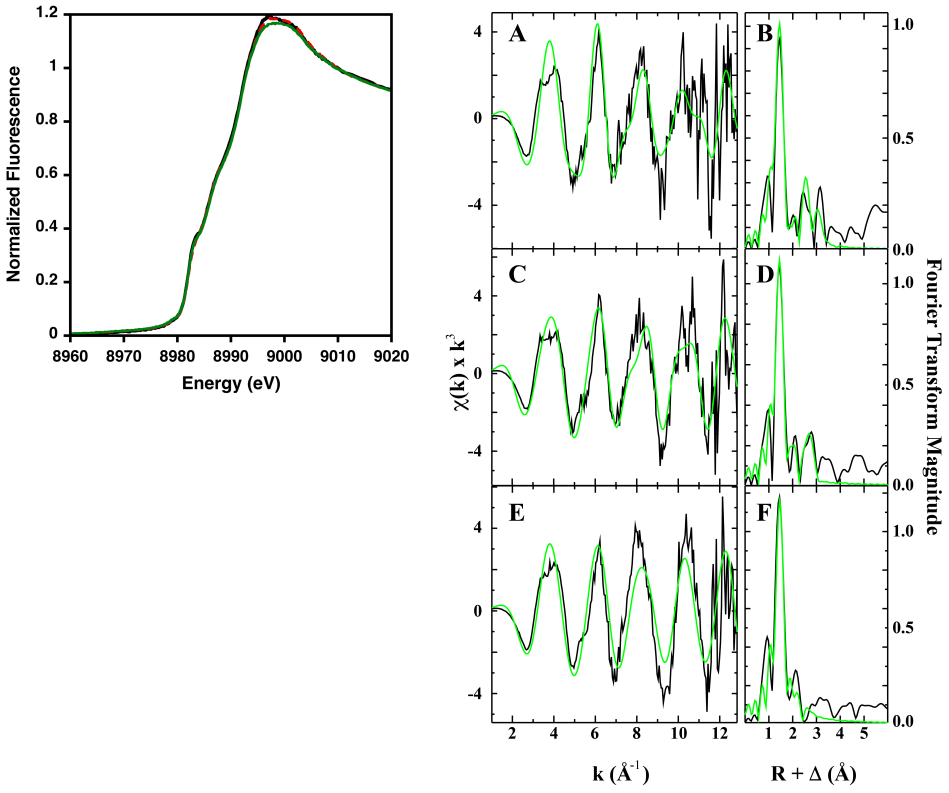

Supporting Tables

Table S1. Stoichiometry of Cu^{2+} binding by *St*CopB. The reported values represent the average and one standard deviation of three or more independent replicates.

Construct	**Cu^{2+} per *St*CopB**
WT-*St*CopB	7.2 ± 1.0
ΔMBD-*St*CopB	1.4 ± 0.2
ΔMBD-*St*CopB_C404A	0.9 ± 0.4
ΔMBD-*St*CopB_H406A	1.0 ± 0.2
ΔMBD-*St*CopB_C404A,H406A	0.3 ± 0.2*

*Although the Cu^{2+} stoichiometry is lower in ΔMBD-StCopB_C404A,H406A than in ΔMBD-StCopB, the EPR signature (and thus, the binding site) is the same for both enzymes.

Table S2. Stoichiometry of Cu^+ binding by *St*CopB. The data represent the average and one standard deviation of three independent replicates.

Construct	**Cu^+ per *St*CopB**
WT-*St*CopB	1.12 ± 0.05
ΔMBD-*St*CopB	1.07 ± 0.09
ΔMBD-*St*CopB_C404A	0.50 ± 0.04
ΔMBD-*St*CopB_H406A	0.83 ± 0.03
ΔMBD-*St*CopB_C404A,H406A	0.66 ± 0.03
ΔMBD-*St*CopB_H406C	2.12 ± 0.15
ΔMBD-*St*CopB_M739A	0.94 ± 0.05

Table S3. Summary of best fit values for WT-*St*CopB Cu EXAFS simulation. EXAFS data were fit over a *k*-range of 1 to 12.8 $Å^{-1}$, for a spectral resolution of 0.13 Å.

Nearest-Neighbor Ligand Environment[a]				**Long-Range Ligand Environment**[a]				
Atom[b]	**R(Å)**[c]	**C.N.**[d]	**σ^2**[e]	**Atom**[b]	**R(Å)**[c]	**C.N.**[d]	**σ^2**[e]	***F'***[f]
S	2.27	3.0	4.73	C	2.74	1.5	3.18	0.19
S	2.47	1.0	4.62	C	4.02	2.0	2.93	

[a] Independent metal-ligand scattering environment

[b] Scattering atoms: S (sulfur), C (carbon)

[c] Average metal-ligand bond length from two independent samples

[d] Average metal-ligand coordination number from two independent samples

[e] Average Debye-Waller factor in $Å^2$ x 10^3 from two independent samples

[f] Number of degrees of freedom weighted mean square deviation between data and fit

Table S4. Summary of best fit values for Cu^{2+}-loaded ΔMBD-*St*CopB total Cu EXAFS simulation. Best fit values were obtained with 4N/O ligands and fits with 3N/O,1S led to high Debye-Waller factors. EXAFS data were fit over a *k*-range of 1 to 12.8 $Å^{-1}$, for a spectral resolution of 0.13 Å.

		Nearest-Neighbor Ligand Environment[a]								**Long-Range Ligand Environment[a]**				
Sample	**Fit[b]**	**Atom[c]**	**R(Å)[d]**	**C.N.[e]**	**s^{2}[f]**	**Atom[c]**	**R(Å)[d]**	**C.N.[e]**	**s^{2}[f]**	**Atom[c]**	**R(Å)[d]**	**C.N.[e]**	**s^{2}[f]**	***F'*[g]**
Δ*St*_CopB	**1**	**O/N**	**1.92**	**2.0**	**1.22**	**O/N**	**2.06**	**2.0**	**2.78**	**C**	**2.99**	**2.0**	**1.95**	**1.41**
										C	**3.43**	**2.0**	**4.85**	
	1.1	O/N	1.95	3.0	6.24	S	2.37	1.0	28.2	C		2.0	1.04	1.61
										C	3.43	2.0	3.55	
C404A	**2**	**O/N**	**1.93**	**2.5**	**1.02**	**O/N**	**2.09**	**1.5**	**1.67**	**C**	**3.01**	**2.0**	**2.86**	**1.20**
										C	**3.31**	**2.0**	**4.15**	
	2.1	O/N	1.93	3.0	3.97	S	2.30	1.0	10.8	C	3.00	2.0	2.26	1.60
										C	3.32	1.5	5.03	
H406A	**3**	**O/N**	**1.93**	**2.5**	**1.05**	**O/N**	**2.10**	**1.5**	**2.50**	**C**	**2.90**	**1.0**	**2.95**	**1.55**
	3.1	O/N	1.94	3.0	3.14	S	2.30	1.0	6.56	C	2.92	1.0	1.70	1.85

[a] Independent metal-ligand scattering environment

[b] Initial number corresponds to sample type while extension number corresponds to number of shells included in the fit.

[c] Scattering atoms: O (oxygen), N (nitrogen), C (carbon)

[d] Average metal-ligand bond length from two independent samples

[e] Average metal-ligand coordination number from two independent samples

[f] Average Debye-Waller factor in $Å^2$ x 10^3 from two independent samples

[g] Number of degrees of freedom weighted mean square deviation between data and fit.

References

1. Delmar JA, Bolla JR, Su CC, Yu EW (2015) Crystallization of membrane proteins by vapor diffusion. *Methods Enzymol* 557:363-392.
2. Buchan DW, Minneci F, Nugent TC, Bryson K, Jones DT (2013) Scalable web services for the PSIPRED Protein Analysis Workbench. *Nucleic Acids Res* 41:W349-W357.
3. Chivian D*, et al.* (2005) Prediction of CASP6 structures using automated Robetta protocols. *Proteins* 61 Suppl 7:157-166.
4. Kim DE, Chivian D, Baker D (2004) Protein structure prediction and analysis using the Robetta server. *Nucleic Acids Res* 32:W526-W531.
5. Wu CC, Rice WJ, Stokes DL (2008) Structure of a copper pump suggests a regulatory role for its metal-binding domain. *Structure* 16(6):976-985.
6. Lanzetta PA, Alvarez LJ, Reinach PS, Candia OA (1979) Improved assay for nanomole amounts of inorganic-phosphate. *Anal Biochem* 100(1):95-97.
7. Smith AT, Barupala D, Stemmler TL, Rosenzweig AC (2015) A new metal binding domain involved in cadmium, cobalt and zinc transport. *Nat Chem Biol* 11(9):678-684.
8. Werst MM, Davoust CE, Hoffman BM (1991) Ligand spin densities in blue copper proteins by Q-band ^{1}H and ^{14}N ENDOR spectroscopy. *J Am Chem Soc* 113:1533-1538.
9. Ankudinov AL, Rehr JJ (1997) Relativistic calculations of spin-dependent X-ray absorption spectra. *Phys Rev B* 56:R1712-R1715.
10. Lieberman RL*, et al.* (2006) Characterization of the particulate methane monooxygenase metal centers in multiple redox states by X-ray absorption spectroscopy. *Inorg Chem* 45:8372-8381.

11. Riggs-Gelasco PJ, Stemmler TL, Penner-Hahn JE (1995) XAFS of dinuclear metal sites in proteins and model compounds. *Coord Chem Rev* 144:245-286.

12. Cotelesage JJ, Pushie MJ, Grochulski P, Pickering IJ, George GN (2012) Metalloprotein active site structure determination: synergy between X-ray absorption spectroscopy and X-ray crystallography. *J Inorg Biochem* 115:127-137.

13. Gerlt JA*, et al.* (2015) Enzyme Function Initiative-Enzyme Similarity Tool (EFI-EST): A web tool for generating protein sequence similarity networks. *Biochim Biophys Acta* 1854(8):1019-1037.

14. Shannon P*, et al.* (2003) Cytoscape: a software environment for integrated models of biomolecular interaction networks. *Genome Res* 13(11):2498-2504.

15. Smith AT, Smith KP, Rosenzweig AC (2014) Diversity of the metal-transporting P_{1B}-type ATPases. *J Biol Inorg Chem* 19(6):947-960.